The ~{311}<136> Recrystallization Texture Component of Non-Oriented Electrical Steels

Leo A.I. Kestens and Tuan Nguyen-Minh
Ghent University, Metal Science and Technology Group
Department of Electromechanics, Systems and Metals Engineering
Technologiepark 46, 9052 Gent, Belgium

Summary

The ~{311}<136> texture component frequently appears in the recrystallization texture of non-oriented electrical steels, either in the texture of the finished product or in an intermediate processing state. This paper presents a brief review of a number of features of this component. First, a precise description of the ~{311}<136> component is presented, as this component is identified under different denominations in the technical literature. Second, it is reviewed what conditions may contribute to the development of the ~{311}<136> component. Surprisingly, it is noticed that ~{311}<136> orientations are omnipresent in the recrystallization texture of extra and ultra-low carbon steels, but only in rare occasions this component emerges as a dominant component of the macroscopic recrystallization texture. A necessary condition for the appearance of the ~{311}<136> component in the macro-texture is the suppression of nucleation and/or growth of the conventional {111} orientations. Third, the mechanisms of nucleation and growth of ~{311}<136> orientations are discussed in terms of the classical theories of oriented nucleation and selective growth. Various elements are listed that may enhance our insight in the origin in the deformed structure and its formation during recrystallization of this remarkable texture component.

1 Introduction

It is well known that texture control is of crucial importance for the magnetic properties of electrical steels, both for Non-Oriented (NO) and Grain-Oriented (GO) grades alike. For GO steels the manufacturing process leading to the very strong Goss texture {110}<001> texture is well-established and still largely based on the Goss procedure that was patented in 1934 [1]. For NO grades, however, the situation is more complicated. Although a large body of literature on texture control in NO steels or texture control in general has been published [2-8], as yet there is not a consensus and widely applied industrial procedure to obtain a sharp θ-fiber texture (<001>//ND), which the target texture for NO electrical steels.
For extra and ultra-low carbon steels, including electrical steels, it is generally accepted that a conventional processing route of (austenitic) hot rolling, cold rolling and (continuous) annealing will

invariably produce a γ-fiber <111>//ND texture. By evacuating as much as possible the C solutes from Fe matrix during the nucleation stage of recrystallization the {111} fiber texture can be strongly enhanced, such as is the case for deep drawable IF steels. Conversely, for obtaining a <001>//ND fiber texture in NO grades, it requires a mechanism to prevent the {111} crystal orientations to nucleate and grow during recrystallization.

In many papers on texture control in NO electrical steel, it is reported that a ~{311}<136> texture component appears after recrystallization as a substitute of or in addition to the conventional γ-fiber. Kestens et al. have indicated the strong relationship between deformation and recrystallization texture, and that the presence of the ~{311}<136> recrystallization texture component is due to the strong preference of crystal orientation to the rotated Cube {001}<110> component after the cross rolling [9]. In a study on the development of (primary and secondary) recrystallization texture on silicon-iron alloys, Homma and Hutchinson have observed the ~{311}<136> component in the primary recrystallization texture, besides the {111}<112> component [10]. The presence of the {311}<136> recrystallization texture on silicon-alloyed ultra-low carbon steel samples after severely cold rolling of 99% thickness reduction is also confirmed by Gobernado et al. [11]. Tomita et al. [12] have reported the presence of the ~{311}<136> recrystallization texture on severely cold rolled Fe-0.3 wt.%Si and Fe-0.3 wt.%Al alloy samples. Although these studies have shown the dependence of recrystallization texture on the deformation state, the mechanism(s) on the development of the ~{311}<136> texture component in cold rolled ferritic materials is not yet fully understood. The potential benefits and the methods to control this recrystallization texture component have not been deeply evaluated yet. Therefore, the main aim of this study is to systematically analyze and account for the formation of the ~{311}<136> recrystallization texture in cold rolled ferritic materials.

2 Description of the ~{311}<136> Texture

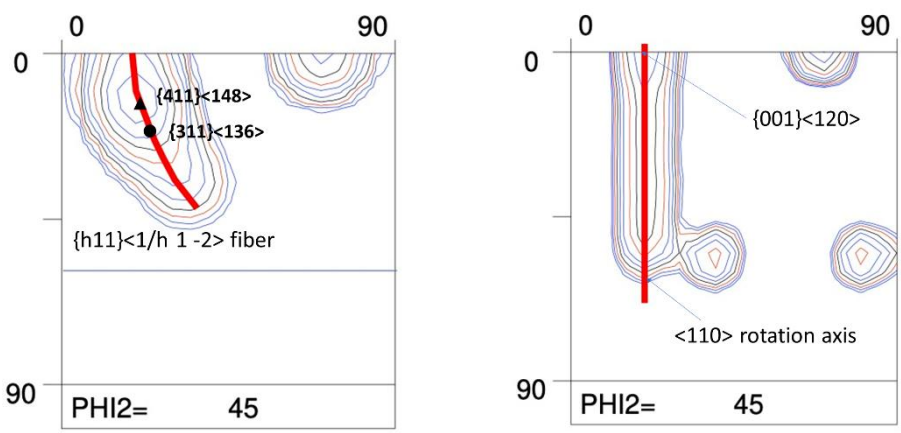

a. b.

Figure n°1: φ_2 = 45° sections of Euler space exhibiting the (a) {h11}<1/h12> fiber with the {311}<136> and {411}<148> components and (b) the fiber obtained by rotating the {100}<012> component around the <110> axis.

The {311}<136> texture component is part of a fiber texture, which according to Homma et al [xx] can be represented by the Miller Indices {h11}<1/h12>. The texture, which is visualized in Fig1a,

starts on the θ-fiber component {100}<012> and in addition to the {311}<136> component, also includes the {411}<148> component. If the θ-fiber component {100}<012> is rotated around the <110> axis, a fiber is generated, which for the lower F values nearly coincides with the {h11}<1/h12>. In practice, a recrystallization texture component might appear in the broad vicinity of the {311}<136> component, i.e. on different locations of the {h11}<1/h12> fiber, or with distributed intensity along this fiber. Therefore, in this paper we will identify these components, of which it might be assumed that they have a common origin, with the generic denomination ~{311}<136>.

3 Circumstantial conditions for the appearance of the ~{311}<136> Component

The ~{311}<136> component may appear after cold rolling and annealing in various types of extra and ultra-low carbon steels. The normal trend of these types of steel is to form a γ-fiber recrystallization texture (<111>//ND). With increasing rolling reduction, the homogeneous intensity distribution along the γ-fiber is altered to a pronounced component in the vicinity of the {111}<112> component and gradually the ODF intensity shifts to the ~{311}<136> component [11]. By Accumulative Roll Bonding (ARB) it is possible to apply very large rolling reductions without continuously thinning the sheet. Fig. 2 shows the texture of an IF steel sheet that was subjected to 10 successive ARB passes of 50% each, producing an accumulated true strain of 6.93 corresponding to a total rolling reduction of 99.9%. Subsequent to cold rolling the sheet was annealed at 750°C for 180 s. It can be observed that the ~{311}<136> component is prominently present in the recrystallization texture, cf. Fig. 3b, whereas the deformation texture, cf. Fig. 2a, is characterized by a very strong α-fiber <110>//RD texture (with an absolute maximum of ~30 mrd on the rotated cube component {001}<110>) and only a weak γ-fiber with an intensity < 2.5 mrd. Furthermore a tiny local maximum on the ~{311}<136> component can be observed in the cold rolled texture of Fig. 2b.

It seems to be a general pattern that the ~{311}<136> component appears in the recrystallization texture when rolling texture is characterized by a strong α-fiber and/or rotated cube component and with virtual absence of the γ-fiber. Similar observations were made by Kestens and Jonas [13]. But even in cases were a strong γ-fiber texture is present such as after cold rolling and annealing of an industrially processed IF steel, cf. Fig. 3a, it appears that in the background intensity also a ~{311}<136> texture component is present; cf. Fig. 3b. The texture of Fig. 3b was derived from the ODF of Fig. 3a by filtering out all orientations that are within a range of 35° from the γ-fiber. It can clearly be seen that in the filtered texture a ~{311}<136> component is present. Hence, it might be the case that the ~{311}<136> component is intricately present among the recrystallized orientations of a cold rolled extra or ultra-low carbon steel, but that it depends on the activation of inhibition factor whether or not the traditional {111} component becomes dominant in the final recrystallization texture. The latter factor is presumably a prerequisite to prevent large scale nucleation of {111} crystal orientations. It remains to be verified whether this is the only possible inhibition factor or also other aspects, such as the addition of grain boundary sensitive alloying elements, may play a role.

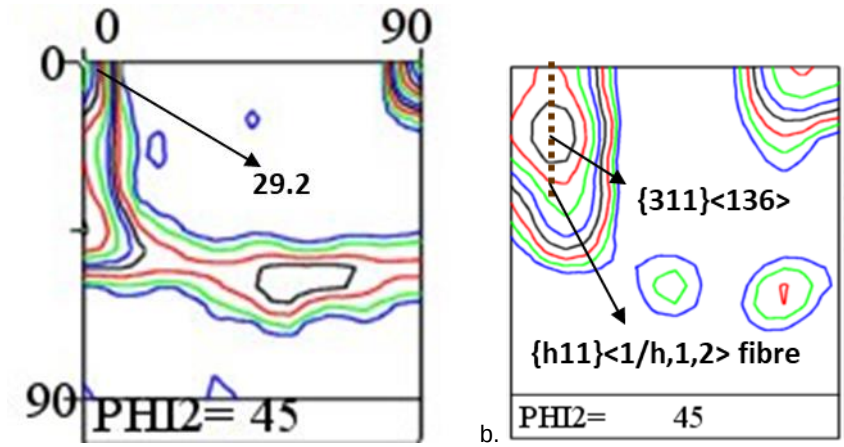

a. b.

Figure n°2: φ_2 = 45° section of the ODF of an IF steel after 10 ARB passes at room temperature with an accumulative rolling of 99.9%; (a) after cold deformation and (b) after recrystallization annealing at 750°C during 180s. (levels: 0.7, 1.0, 1.4, 2.0, 2.8, 4.0, 5.6, 8.0, 11, 16)

4 On the Formation Mechanism of the ~{311}<136> Component

Both oriented nucleation and selective growth theories have been reported to explain the appearance of the ~{311}<136> recrystallization component.

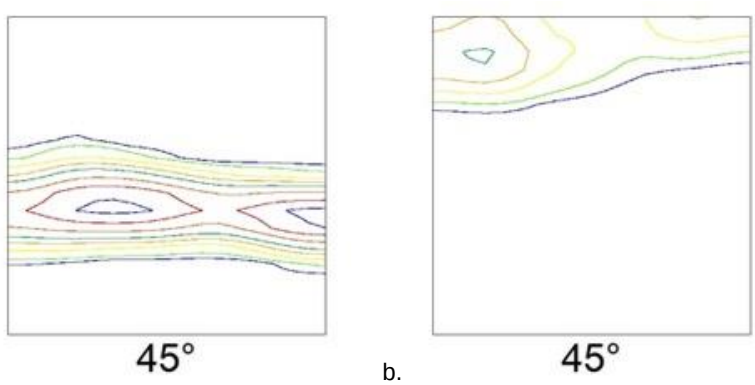

a. b.

Figure n°3: φ_2 = 45° section of the ODF of (a) a commercially processed cold rolled and annealed IF steel; (b) texture obtained from (a) by removing all orientations within 35° from the γ-fiber (levels: 1.0, 2.0, 4.0, 8.0, 11, 14, 18)

4.1 Oriented Nucleation Arguments

Oriented nucleation of specific crystal orientations requires that these orientations are present in the deformation texture in sufficient frequency and a mechanism that favors nucleation of same orientations in the early stages of recrystallization. In an elegant experiment on cold rolled bicrystals of slightly misoriented rotated cube orientations Homma et al [14] have observed ~{311}<136> orientations among the first nuclei during recrystallization. Quadir and Duggan [15] and Gobernado et al. [11] have confirmed the presence of ~{311}<136> oriented deformation bands in deformed α-fiber grains after a severe cold rolling reduction of 95% in the case of Quadir and Duggan [15] and after 60% cross rolling in the report of Gobernado et al. [11]. These observations were restricted to the identification of local ~{311}<136> bands on orientation contrast maps of sufficient resolution, though the ~{311}<136> component did not appear, not even as a local maximum, in the cold rolling texture of these materials. However, the data gathered on ARB processed material to extremely high levels of rolling reduction (99.9 %), cf. Fig. 2b, do confirm that in such exceptional cases a ~{311}<136> component can be observed in the macrotexture, albeit as a tiny local maximum. Unfortunately, the ARB material of Fig. 2b could not be investigated by EBSD because the defect density was far too high.

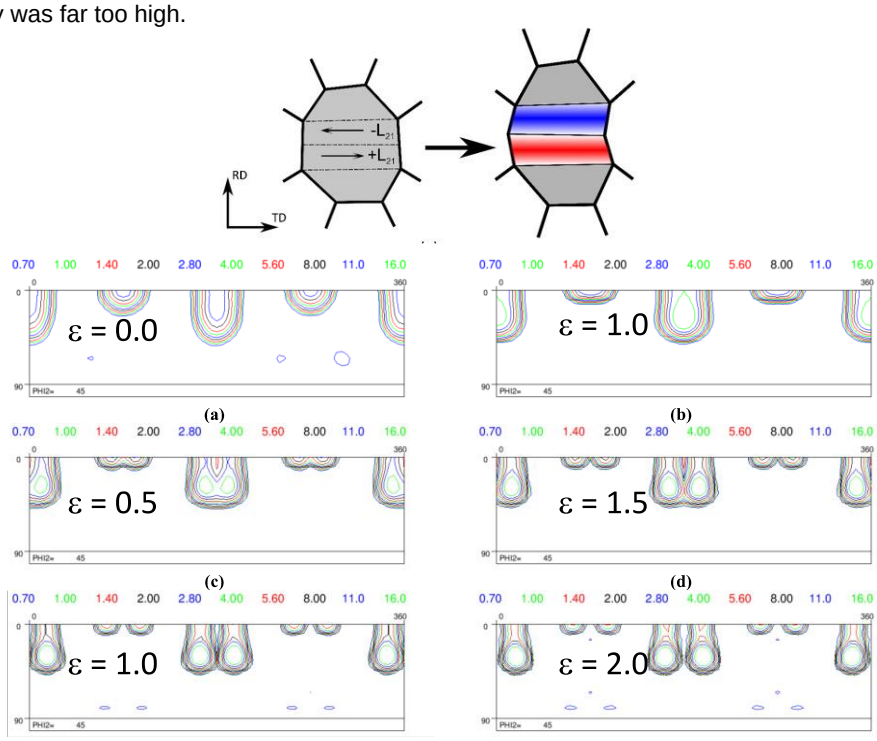

Figure n°4: The effect of a non-zero shear component L21 to the plane strain velocity gradient tensor on the orientation change of an initial α-fiber for various levels of strain.

As local orientation gradients are responsible for the introduction of the ~{311}<136> component in α-fiber deformed grains the question remains why only this component stands out among plenty of other local rotation events associated with the fragmentation of the initial hot band grains and a

fortiori why only these ~{311}<136> are selected for nucleation. By applying a conventional Full constraint Taylor model Nguyen-Minh [16] has demonstrated that by adding a non-zero L_{21} shear component to the plane strain velocity tensor of rolling, the initial α-fiber orientations rotate towards the ~{311}<136> component after medium to high strains, cf. Fig. 4. However, as yet the precise origin of the local constraints that impose such a local L_{21} shear component remains unknown. It requires an accurate crystal plasticity fragmentation model to unravel the detailed mechanism of strain localization. Perhaps the full-field spectral solver approach with adaptive remeshing that was recently proposed by Saghediana et al. [17] may offer more in-depth insight on the origin of ~{311}<136> oriented deformation bands.

4.2 Selective Growth Arguments

In BCC alloys selective growth is generally associated with the presumed enhanced mobility of grain boundaries that carry a <110>26.5° crystal misorientation between the neighboring grains [18]. Urabe and Jonas [19] have extended the <110>26.5° condition for selective growth to a more general {110} plane matching condition, whereby it is required that the growing nucleus and the deformed matrix grain share a common {110} plane within a certain given tolerance such as e.g. 5°. When Kestens and Jonas [13, 20] applied the {110} plane matching criterion on the deformation texture of a 95% cold rolled ultra-low carbon steel, it was observed that the strong α-fiber rolling texture was converted to a {h11}<1/h12> texture implying that the orientations of the {h11}<1/h12> fiber comply with the plane matching condition for the given deformation texture.

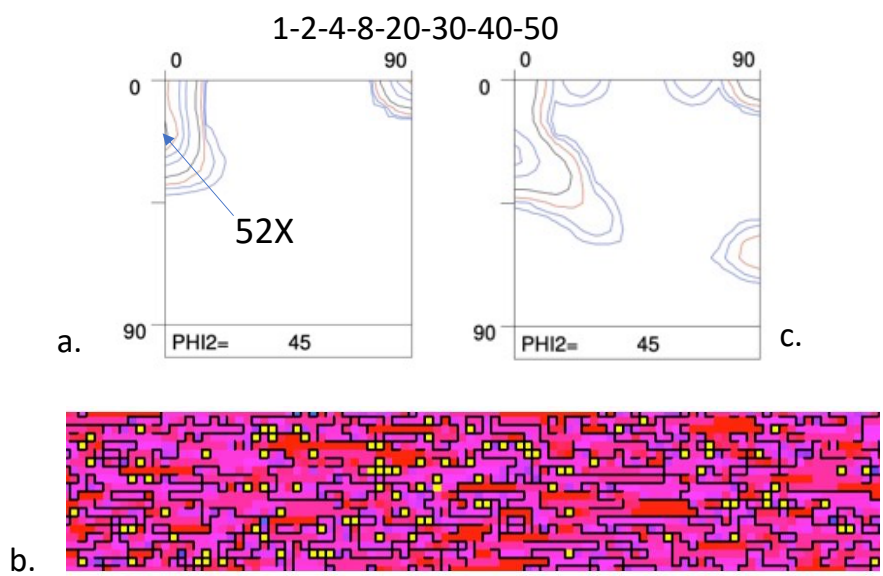

*Figure n°5: (a) Simulated cold rolling texture obtained by applying the ALAMEL model to a set of 2,000 discrete orientation within a 16° tolerance from the rotated cube orientation; (b) grid of 100*20 pixels - to each of the pixels an orientation of the deformation texture was randomly assigned; yellow pixels are fully surrounded by HAGBs; (c) texture corresponding to the tallow pixels.*

Orientation pinning is another, perhaps less controversial mechanism of selective growth. As it is generally accepted that Low Angle Grain Boundaries (LAGBs) exhibit a reduced mobility, it is reasonable to assume that for a deformation texture that is dominated by a strong single component only a small minority of nucleus orientations will have the potential to grow into the single component deformation texture, namely the nuclei that are surrounded with a super-critical area of highly mobile High Angle Grain Boundaries (HAGBs). This principle was applied in the following model whereby first a plane strain rolling reduction of 80% was simulated with the ALAMEL crystal plasticity model [21] for a set of 2,000 initial orientation within a range of less than 16° from the rotated cube component. Hereby {110}+{112} pencil glide was assumed with equal critical resolved shear stresses on all slip systems. The simulated rolling texture, cf. Fig. 5a, exhibits a very strong α-fiber with a maximum of 52 mrd in the vicinity of the {113}<110> component. Subsequently, the 2,000 crystal orientations were randomly assigned to a grid of 100*20 square pixels, mimicking a 2D microstructure with random topology, cf. Fig. 5b. Assuming that each of the crystal orientations of the grid represents a physical grain it is possible to extract the grains that are fully surrounded by HAGBs, corresponding to the yellow grains of Fig. 5b (in this case it was assumed that HAGBs exceed a misorientation of 20°). It can be observed that the texture associated with the yellow grains, cf. Fig. 5c, still exhibits a maximum on the {113}<110> component, but additionally there is also a local maximum on the {001}<120> component on the {h11}<1/h12> fiber and in general the α-fiber has widened somewhat. Thus, it can be concluded that under the prevailing modeling assumptions the orientation pinning principle cannot explain the appearance of the ~{311}<136> component, although the principle does not exclude the {h11}<1/h12> fiber from the set of pinning free orientations.
As a concluding remark it needs to be mentioned that oriented nucleation and selective growth arguments are not mutually exclusive and may even enhance each other; i.e. oriented nucleation and selective growth may occur simultaneously and equally contribute to the formation of the recrystallization texture.

5 Conclusion

In this paper some considerations were presented about the features of the ~{311}<136> component frequently appearing in the recrystallization texture of non-oriented electrical steels. A precise description was given of the {h11}<1/h12> fiber to which the {311}<136> component belongs together with the adjacent {411}<148> component. It was emphasized that the ~{311}<136> component is omnipresent in the recrystallization texture of (ultra-)low carbon steels, albeit as a tiny minority component if the dominant {111} component is not inhibited in the recrystallization process. The presence of a strong α-fiber (with maximum on the rotated cube component) together with the absence of a strong γ-fiber in the rolling texture enhances the development of the ~{311}<136> component and suppresses the formation of a γ-fiber during recrystallization. With regard to the mechanism of ~{311}<136> recrystallization both oriented nucleation and selective growth arguments can be formulated. ~{311}<136> oriented grains are observed in deformation bands within α-fiber grains of the deformed structure, which can be explained by local accommodation of L_{21} shear. With regard to selective growth it was noticed that if the well-known <110>26.5° selection criterion of enhanced grain boundary mobility is extended to a more general {110} plane matching criterion the α-fiber of the rolling texture is converted to a {h11}<1/h12> fiber. Also the role of the orientation pinning mechanism was reviewed.

6 References

[1] Goss, N.P., Electrical sheet and method and apparatus for its manufacture and test. *US Patent*, **1934**, *1965559A*.
[2] Kestens, L.; Jacobs, S., Texture control during the manufacturing of nonoriented electrical steels. *Texture Stress Microstruct.* **2008**, *2008*, pp.
[3] Doherty, R.D.; Stojakovic, D.; Landgraf, F.J.G.; Kalidindi, S.R., Retention of the 〈001〉 fiber texture for Fe-Si electric motor steels. *Mater Sci Forum* **2007**, *550*, pp. 497-502.
[4] Stojakovic, D.; Doherty, R.D.; Kalidindi, S.R.; Landgraf, F.J.G., Thermomechanical processing for recovery of desired 〈001〉 fiber texture in electric motor steels. *Metall Mat Trans A Phys Metall Mat Sci* **2008**, *39*, pp. 1738-1746.
[5] Tomida, T., A new process to develop (100) texture in silicon steel sheets. *J Mater Eng Perform* **1996**, *5*, pp. 316-322.
[6] Tomida, T., Decarburization of 3%Si-1.1%Mn-0.05%C steel sheets by silicon dioxide and development of {100}<012> texture. *Mater. Trans.* **2003**, *44*, pp. 1096-1105.
[7] Park, J.Y.; Oh, K.H.; Ra, H.Y., Microstructure and crystallographic texture of strip-cast 4.3wt%Si steel sheet. *Scr. Mater.* **1999**, *40*, pp. 881-885.
[8] Zapuskalov, N., Effect of coiling operation on strip quality of 4.5% Si steel in twin-roll casting process. *ISIJ Int* **1999**, *39*, pp. 463-470.
[9] Kestens, L.; Jonas, J.J.; Van Houtte, P.; Aernoudt, E., Orientation selective recrystallization of nonoriented electrical steels. *Metall. Mater. Trans. A* **1996**, *27*, pp. 2347-2358.
[10] Homma, H.; Hutchinson, B.; Kubota, T., The production mechanism of extensively sharp Goss orientation in HI-B material. *J. Magn. Magn. Mater.* **2003**, *254–255*, pp. 331-333.
[11] Gobernado, P.; Petrov, R.; Ruiz, D.; Leunis, E.; Kestens, L.A.I., Texture evolution in Si-alloyed ultra low-carbon steels after severe plastic deformation. *Adv. Eng. Mater.* **2010**, *12*, pp. 1077-1081.
[12] Tomita, M.; Inaguma, T.; Sakamoto, H.; Ushioda, K., Recrystallization behavior and texture evolution in severely coldrolled Fe-0.3mass%Si and Fe-0.3mass%Al alloys. **2017**, *57*, pp. 921-928.
[13] Kestens, L.; Jonas, J.J., Modeling texture change during the static recrystallization of interstitial free steels. *Metall. Mater. Trans. A* **1996**, *27*, pp. 155-164.
[14] Homma, H.; Nakamura, S.; Yoshinaga, N., On {h,1,1}<1/h,1,2>, the recrystallisation texture of heavily cold rolled BCC steel. *In Proceedings of the The 2nd International Conference on Recrystallization and Grain Growth*, France, **2004**, Materials Science Forum, *467-470*, pp. 269-274.
[15] Quadir, M.Z.; Duggan, B.J., Deformation banding and recrystallization of α fibre components in heavily rolled IF steel. *Acta Mater.* **2004**, *52*, pp. 4011-4021.
[16] Nguyen-Minh, T., Crystallographic texture control in a non-oriented electrical steel by plastic deformation and recrystallization. *PhD Thesis*, **2021**, *Delft University of Technology*, Delft - The Netherlands.
[17] Sedighiani, K.; Shah, V.; Traka, K.; Diehl, M.; Roters, F.; Sietsma, J.; Raabe, D., Large-deformation crystal plasticity simulation of microstructure and microtexture evolution through adaptive remeshing. *Int. J. Plast.* **2021**, *146*, pp.
[18] Ibe, G.; Lücke, K., Growth selection during recrystallization of single crystals. **1966**, pp.
[19] Urabe, T.; Jonas, J.J., Modeling Texture Change during the Recrystallization of an IF Steel. *ISIJ Int.* **1994**, *34*, pp. 435-442.
[20] Kestens, L.; Jonas, J.J., Modelling Texture Change during the Static Recrystallization of a Cold Rolled and Annealed Ultra Low Carbon Steel Previously Warm Rolled in the Ferrite Region. *ISIJ Int.* **1997**, *37*, pp. 807-814.
[21] Van Houtte, P.; Li, S.; Seefeldt, M.; Delannay, L., Deformation texture prediction: From the Taylor model to the advanced Lamel model. *Int. J. Plast.* **2005**, *21*, pp. 589-624.